HHS Public Access

Author manuscript

Biotechnol Bioeng. Author manuscript; available in PMC 2018 January 23.

Published in final edited form as:

Biotechnol Bioeng. 2016 September ; 113(9): 2020–2032. doi:10.1002/bit.25950.

A Reductionist Metastasis-on-a-Chip Platform for In Vitro Tumor Progression Modeling and Drug Screening

Aleksander Skardal[1,2,3], **Mahesh Devarasetty**[1,2], **Steven Forsythe**[1], **Anthony Atala**[1,2], and **Shay Soker**[1,2,3]

[1]Wake Forest Institute for Regenerative Medicine, Wake Forest School of Medicine, Medical Center Boulevard, Winston-Salem, North Carolina

[2]Virginia Tech-Wake Forest University School of Biomedical Engineering and Sciences, Wake Forest Baptist Health, Medical Center Boulevard, Winston-Salem, North Carolina

[3]Department of Cancer Biology, Wake Forest School of Medicine, Medical Center Boulevard, Winston-Salem, North Carolina 27157

Abstract

Current animal and 2-D cell culture models employed in metastasis research and drug discovery remain poor mimics of human cancer physiology. Here we describe a “metastasis-on-a-chip” system allowing real time tracking of fluorescent colon cancer cells migrating from hydrogel-fabricated gut constructs to downstream liver constructs within a circulatory fluidic device system that responds to environmental manipulation and drug treatment. Devices consist of two chambers in which gut and liver constructs are housed independently, but are connected in series via circulating fluid flow. Constructs were biofabricated with a hyaluronic acid-based hydrogel system, capable of a variety of customizations, inside of which representative host tissue cells were suspended and metastatic colon carcinoma tumor foci were created. The host tissue of the constructs expressed normal epithelial markers, which the tumor foci failed to express. Instead, tumor regions lost membrane-bound adhesion markers, and expressed mesenchymal and proliferative markers, suggesting a metastatic phenotype. Metastatic tumor foci grew in size, eventually disseminating from the intestine construct and entering circulation, subsequently reaching in the liver construct, thus mimicking some of the migratory events observed during metastasis. Lastly, we demonstrated the ability to manipulate the system, including chemically modulating the hydrogel system mechanical properties and administering chemotherapeutic agents, and evaluated the effects of these parameters on invasive tumor migration. These results describe the capability of this early stage metastasis-on-a-chip system to model several important characteristics of human metastasis, thereby demonstrating the potential of the platform for making meaningful advances in cancer investigation and drug discovery.

Correspondence to: A. Skardal, telephone: 336-713-1649; fax: 336-713-7290; askardal@wakehealth.edu.

Conflict of interest: The authors have no conflicts of interest to disclose.

Supporting Information

Additional supporting information may be found in the online version of this article at the publisher’s web-site.

Keywords

cancer; in vitro models; organs-on-a-chip; diagnostics; hydrogel

Introduction

Despite advances in medical treatments, cancer metastasis is still not well understood; in particular (i) the mechanisms behind activation of tumor cell growth and malignancy, (ii) how these mechanisms impact the logistics and kinetics of metastasis, and (iii) the role that the microenvironment plays in regulating these phenomena (Fidler et al., 2007; Langley and Fidler, 2007). While cancer research continues to progress, in recent years it has been limited due to the inability to accurately model tumor progression and metastasis in a controlled environment. Animal models allow only limited manipulation and study of the mechanisms at play, and are not necessarily predictive of results in humans. On the other hand, in vitro methods, such as traditional 2-D cultures, fail to recapitulate the 3-D microenvironment of in vivo tissues (Kunz-Schughart et al., 2004). Drug diffusion kinetics vary dramatically, drug doses effective in 2-D are often ineffective when scaled to patients, cellular phenotypes can differ, and cell-cell/cell-matrix interactions are inaccurately modeled (Drewitz et al., 2011; Ho et al., 2010; Skardal et al., 2015a). These limitations result in “top level” drug candidates often reaching clinical trials and failing because they have not been tested in accurate human-based models. Instead, platforms that include 3-D tissue constructs, or organoids, created using 3-D biomaterial systems and human-derived cells offer a better solution for mimicking native physiology, modeling diseases, and performing drug screening (Benam et al., 2015; Polini et al., 2014). Our laboratory has extensive experience with fabrication and maintenance of tissue constructs of various types, including liver and intestine, and has been a part of the development and implementation of a number of hydrogel technologies to do so (Murphy et al., 2013; Skardal et al., 2010a,b,c,d, 2012; Zhang et al., 2008). These types of approaches to hydrogel biofabrication, which in our case often employ customized hyaluronic acid hydrogels with an incredible versatility in regenerative medicine and tissue engineering applications (Allison and Grande-Allen, 2006; Burdick and Prestwich, 2011; Prestwich, 2007, 2008; Prestwich and Kuo, 2008), can be used to create engineered 3-D human-specific models that can more accurately recapitulate human physiology and disease.

In the case of metastasis research, there is a lack of in vitro models that distinguish between the primary tumors and the distant metastatic growth. Here we describe the initial implementation of multiple 3-D tissue constructs within a closed fluidic system that allows control over the environment and investigation of mechanisms of metastasis at play across two distinct tissues in one platform—a “metastasis-on-a-chip” (MOC). The introduction of tumor foci within host tissue constructs is a concept that to date has not been sufficiently employed. This nexus of tissue engineering with micro-scale devices, paired with potential for real time live imaging, results in a powerful investigative and diagnostic tool. By providing flow through the fluidic device tissue construct system, we can study the dissemination of colon carcinoma cells from the gut construct into circulation, after which metastatic cells can attach and invade the liver construct downstream. The microfluidic

model is one of the first in vitro models of metastasis recapitulating migration from a 3-D originating tissue to a 3-D target tissue. This is notable and novel because the phenotype of cells in the originating malignant tumors and metastases can vary significantly—for example, resulting in varying levels of invasiveness due to matrix metalloproteinase (MMP) secretion and stem cell-like gene expression (Franci et al., 2013; Karakiulakis et al., 1997)—making the ability to study tumors in various settings, their microenvironments, and during migration extremely informative.

Materials and Methods

Cell Culture

Human colon carcinoma cells (HCT-116, transfected previously with red fluorescent protein [RFP]), human intestine epithelial cells (INT-407), and human hepatoma cells (HepG2) were expanded in 2-D on tissue culture plastic using 15 cm tissue-treated dishes until 90% confluence with Dulbecco's Minimum Essential Medium (DMEM, Sigma, St. Louis, MO), containing 10% fetal bovine serum (FBS, Hyclone, Logan, UT). Cells were detached from the substrate with Trypsin/EDTA (Hyclone) and resuspended in media before use in further studies.

Fluidic Device Fabrication and Fluid Circuit Operation

Each device consists of 2 circular chambers (10 mm diameter, 3 mm thick), each accessible via its own fluidic channel with an individually addressable inlet and outlet. These structures are fabricated using conventional soft lithography, replica molding, and layer-by-layer stacking (Fig. 1B; Skardal et al., 2015b; Xia and Whitesides, 1998). Briefly, inverted chamber/channel structures were produced with 3D printing (Zprinter 450, Z Corp., Rock Hill, SC) and used as molds. Polydimethylsiloxane (Sylgard 184, Dow Corning Corporation, Midland, MI) was mixed thoroughly with its curing agent and degassed under vacuum in a desiccation chamber before being poured directly on the mold and cured at 60°C for 60 min. Following curing, the device was isolated from the unnecessary material using a razor and removed from the mold. After cleaning with ethanol, the layers of PDMS were stacked and ready for tissue construct integration. Following introduction of constructs, a flat piece of PDMS containing inlet and outlet ports was used to cover the chambers and channels and the whole device was sealed and clamped. Fluidic connections were made using stainless steel catheter couplers (Instech Laboratories, Plymouth Meeting, PA) and Sylastic tubing (Corning, Corning, NY), which interfaced with the PDMS device through pre-fabricated accessible ports. Each set of chambers were connected to a micro-peristaltic pump and media reservoir for driving flow through the circuit, thereby acting as a simplified circulatory system (Fig. 1C,D).

Hydrogel Tissue Construct Formation

Constructs were formed using a thiolated hyaluronic acid, thiolated gelatin, and polyethylene glycol diacrylate (PEGDA)-based hydrogel system (ESI-BIO, Alameda, CA). Thiolated HA and gelatin components were dissolved at 1% w/v each in water containing 0.1% w/v photoinitiator (2-Hydroxy-4′-(2-hydroxyethoxy)-2-methylpropiophenone, Sigma, St. Louis, MO), and mixed with a 2% w/v linear polyethylene glycol diacrylate crosslinker

solution in a 2:2:1 ratio by volume. For construct formation, the hydrogel-precursor solution was used to resuspend cells at a cell density of 10×10^6 cells/mL. The primary site gut constructs containing colon carcinoma tumor foci were formed using Int-407 intestine epithelial cells and red fluorescent protein (RFP)-labeled HCT-116 colon carcinoma cells, combined in a 10:1 ratio by cell number. The secondary site liver constructs were formed using HepG2 liver cells only. Cell suspensions in the hydrogel precursors were pipetted in 25 μL aliquots into the appropriate device chambers, after which construct photopolymerization was achieved using exposure to UV light (Fig. 1A). Experiments were conducted using DMEM as described above.

Metastasis-on-a-Chip Culture

Dual tissue construct culture onboard the MOC devices was performed after constructs had been formed in each of the device chambers, and the device pieces were sealed and clamped together. Sylastic tubing was used to connect MOCs, media reservoirs, and bubble traps to a MP2 Precision micro-peristaltic pump (Elemental Scientific, Inc., Omaha, NE). Additional tubing further connects the pump to the device and back to the reservoirs, forming multiple closed parallel circuits. At the start of culture, 4 mL of media (DMEM) was placed in each reservoir after which fluid flow was initiated by the micro-peristaltic pump. Media flow was initiated and maintained at a rate of 5 μL/min throughout the experiment. Devices were operated continuously, with media changes occurring if the pH level of the media reservoir dropped, indicated by the phenol red component in the media. During media changes, spent media was removed from the system, placed into a conical tube, and centrifuged to avoid losing any tumor cells that might have entered circulation. Spent media was aspirated and replaced with fresh DMEM. The conical tubes were treated as if there was a cell pellet present—resuspension by pipetting media up and down—and this media and any cells present were returned to media reservoir. During MOC system culture, constructs and presence of fluorescent RFP-labeled tumor foci were documented over time by microscopy. Composite images were taken of the primary construct on days 1, 4, 9, 11, 14, and 17, and secondary site following primary construct tumor cell dissemination on days 14, 18, 20, and 24, in which the constructs were imaged with light microscopy and epifluorescence at 594 nm to analyze the progression of the RFP-labled HCT-116 cells within the non-fluorescent host liver constructs. Percentage of RFP-labeled HCT-116 tumor cell content was measured using a custom MatLab segmentation script (Supporting File 1). Subsets of HCT-containing constructs were fixed on day 21 for histological analysis.

This MOC culture methodology and tracking was the repeated with SW480 colon carcinoma cells in place of the HCT-116 cells. SW480 cells are notably less metastatic than HCT-116 cells, and would potentially offer the ability to model the system using a less malignant tumor population. For tracking purposes, SW480 cells were labeled using Vybrant DiI fluorescent dye (ThermoFisher, Waltham, MA) as directed by the manufacturer’s directions.

Immunohistochemistry and Phenotype Quantification

Constructs were fixed with 4% paraformaldehyde for 1 h, dehydrated with graded ethanol washes followed by xylene, embedded in paraffin, and sectioned at 5 μm. For IHC, all incubations were carried out at room temperature unless otherwise stated. Slides were

warmed at 60°C for 1 h to increase bonding to the slides. Antigen retrieval was performed on all slides and achieved with incubation in Proteinase K (Dako, Carpinteria, CA) for 5 min. Sections were permeabilized by incubation in 0.05% Triton-X for 5 min. Non-specific antibody binding was blocked by incubation in Protein Block Solution (Abcam, Cambridge, MA) for 15 min. Sections were incubated for 60 min in a humidified chamber with the primary ZO-1 (raised in rabbit, cat. # 61–7300, Invitrogen), β-catenin (raised in rabbit, cat. # 71–2700, Invitrogen), vinculin (raised in mouse, cat. # V9264, Sigma Aldrich), N-cadherin (raised in mouse, 610921, BD Biosciences), PCNA (raised in rabbit, cat. # 07–2162, Millipore), and MMP 9 (raised in rat, cat. # ab38898, Abcam) all at 1:200 dilutions in antibody diluent (Abcam).

Following primary incubation, slides were washed 3 times in PBS for 5 min. Samples were then incubated for 1 hr with anti-rabbit, or anti-mouse Alexa Fluor 488 secondary antibodies (Invitrogen) as appropriate in antibody diluent (1:200 dilution). Cells were counterstained with DAPI for 5 min, and washed 3 times with 1 × PBS prior to fluorescent imaging. Negative controls were performed in parallel with the primary antibody incubations and included incubation with blocking solution in place of the primary antibody. No immunoreactivity was observed in the negative control sections. Samples were imaged by epifluorescence using excitation band filters with central excitation wavelengths 380, 488, and 594 nm with a Leica DM 4000B upright microscope (Leica Microsystems, Buffalo Grove, IL).

Images captured of tissue sections stained with the markers described above were used to quantify expression of the markers in HCT116 cells. The percentage of HCT116 cells expressing a particular marker was calculated by counting the total number of HCT116 cells present in a given image, identified by red fluorescence from the RFP tag. Positive expression of a given marker within the HCT116 subset of cells was then counted. Percentage of expression within the RFP+ HCT116 population was then determined by dividing the number of positively expressing cells by the number of total HCT116 cells and multiplying by 100%. For ZO-1, β-catenin, and vinculin, positive expression was defined as readily visible expression associated with the cell membrane, indicating a traditionally epithelial-like morphology. For N-cadherin, MMP 9, and PCNA, expression was considered positive if the stain was present inside the cell.

Construct Environmental Stiffness Manipulation and Migration Tracking

To assess the influence of the physical tumor microenvironment parameters on tumor cell migration, a variation of the constructs described above were formed. Instead of encapsulating homogenously mixed cells throughout the hydrogel, 3-D construct volumes were formed first, after which a volume of 5 μL HCT-116 cells in hydrogel precursor solution was pipetted into the center of the construct space and polymerized in place by a 1 second exposure to UV light. This fabrication scheme resulted in outer construct zones, inside of which distinct tumor zones resided. Construct and tumor zone elastic moduli were modulated by swapping of the linear PEGDA crosslinker molecule (3.4 kDa MW) with a 4-arm PEG-acrylate molecule (10 kDa MW, Creative PEGWorks, Winston-Salem, NC) or 8-arm PEG-acrylate crosslinker molecule (10 kDa MW, Creative PEGWorks) to generate

stiffer hydrogels. Construct constructs were fabricated in 2 primary conditions: condition 1–stiff (8-arm crosslinker) HCT-116 tumor foci inside of a soft environment (linear crosslinker); or condition 2–soft (linear crosslinker) HCT-116 tumor foci inside of a stiff environment (8-arm crosslinker). Constructs were maintained as described above using DMEM. After 7 days, constructs were fixed, and are imaged using a Leica TCS LSI macro-confocal microscope. Z-stacks of 150 μm were taken of each construct near the top of the initial tumor zone, from which maximum projections (2-D compressed image) were obtained.

Drug Treatments and Assessment of Migration

To investigate the likely mechanism of migration within the MOC system, and verify whether the tumor cells were susceptible to drug intervention, the effectiveness of the anti-matrix metalloproteinase drug Marimastat was tested using the multi-zone migration model described above. Tumor constructs were created once more, using the condition 2 described above (soft tumor, stiff tissue), in which, as described in the results, HCT-116 cells displayed heightened migration behavior. One half of the prepared systems received normal DMEM, while the other half received 50 μM Marimastat (Sigma) in DMEM. The drug-containing media was pHed to physiological pH to ensure that any pH changes due to the drug were not confounding results. Fluorescent and brightfield overlay images were captured on day 3, day 7, and day 10, from which distances of migration of cells out of the tumor were determined over time using ImageJ software.

Additionally, constructs were subjected to the anti-proliferative drug 5-fluorouracil (5-FU), a drug commonly employed in cases of colorectal cancer. HCT-116 foci were maintained inside the gut constructs for 14 days after which they were subjected to DMEM containing 0, 1, 10, or 100 mM 5-FU for 48 h. Constructs were then transferred to wells with 150 μL fresh media containing 15% MTS assay reagent (Promega, Madison, WI) and incubated at 37°C for 1 h. After 1 h, 100 μL aliquots of the media-reagent mix were transferred to a clear-bottom 96-well plate and assessed for absorbance at 490 nm on a tunable plate reader. Absorbance is proportional to mitochondrial metabolism in the cells.

Statistical Analysis

The data are generally presented as the means of number of replicates ± the standard deviation. All experiments were performed with $n = 3$ or higher. Values were compared using Student's t-test (2-tailed) with two sample unequal variance, and $P < 0.05$ or less was considered statistically significant.

Results

Metastatic Tumor Constructs in the MOC System Migrate From Gut to Liver

Constructs were fabricated by cell encapsulation (Fig. 1A) using a thiolated hyaluronic acid (HA) and gelatin-based hydrogel, commercially available as HyStem that has been employed extensively in tissue engineering and regenerative medicine (Burdick and Prestwich, 2011; Prestwich, 2011). Examples of applications include 3-D culture (Skardal et al., 2012; Zhang et al., 2008), tumor models (Skardal et al., 2010a), and biofabrication

techniques (Skardal et al., 2010b,c,d). Modulation of the crosslinker geometry (linear, 4-arm, and 8-arm) can be used for controlling construct elastic modulus, which will be described at a later point. In the sealed fluidic devices (Fig. 1B–D), the hydrogel-based gut-tumor constructs and liver constructs were formed and then maintained under circulating flow. Over time in culture, RFP-labeled HCT-116 cells comprising the tumor foci within the primary gut constructs proliferated, and the RFP-positive tumor regions grew in size until dissemination from the construct into the circulating media flow, typically around day 14 of culture (Fig. 2A). After entering the circulating media flow, RFP-labeled cells were able to reach the secondary liver construct constructs, and invade via multicellular aggregates (Fig. 2B). Tumor cells in the liver construct then continued to proliferate, with tumor foci growing in size. Time from dissemination to reaching the liver was variable, but typically occurred within 2–3 days following entrance into the circulation. Percentage of construct area occupied by the fluorescent tumor cells was determined by assessing composite images from various locations at each construct using custom MatLab segmentation code (Supporting File 1). These results (Fig. 2D) further demonstrated the trend of tumor growth in the primary construct, and later colonization and growth in the secondary construct. Initially, fluorescent HCT-116 cells in the intestine constructs occupied a low percentage of the field of views assessed at day 1 (less than 0.05%), but proliferated over time, resulting in nearly 20% of field of views assessed (Fig. 2D, black solid line). Importantly, these data also show the initiation and continuation of tumor growth at the metastatic downstream site following colonization. In this second growth curve (Fig. 2D, black dashed line), zero HCT-116 cells were observed on day 14, which is when we first observed tumor cells entering circulation, but they quickly establish a foothold by day 18 and rapidly increase in number and tumor percentage over the following 6 days.

Additionally, SW480 cells were employed in a similar manner to assess how a less metastatic colon carcinoma cell population with less invasive tendencies would behave in the system. DiI labeling resulting in a fluorescent signal from the cells that was sufficient for the tracking approach employed. It should be noted that after too much proliferation, the fluorescent probes of DiI (or DiO and DiD) labeling solutions can become too diffuse to continue to provide an accurate and strong signal. Fortunately, this was not encountered during the duration of the experiment. In general, proliferation and quantification of SW480 cells over time in the primary gut construct was somewhat reduced compared to that of the HCT-116 cells. The cells increased in area covered by red fluorescence, (Fig. 2C), and this observation was mirrored by the quantified results although the trend was more flat than HCT-116 proliferation (Fig. 2D, blue solid line). However, SW480 cells were never observed disseminating out from the primary construct; they appeared always to reside within the construct borders. With no dissemination, there was no indication of red fluorescence in the downstream site (Fig. 2D, blue dashed line). This second set of migration results suggests that the SW480 cells, which are less metastatic than HCT-116 cells, are less able to “metastasize” within the MOC. Being able to model both less malignant, but positive primary tumor growth and metastatic-like migration from one site to another are both important capabilities for a tumor model system.

Metastasized Colon Carcinoma Tumor Foci Display Markers of Tumorigenic and Mesenchymal Phenotype

Intestine constructs containing primary tumor foci and liver constructs containing metastases were fixed and processed to generate tissue sections for immunostaining protocols. The intestine epithelial regions (Fig. 3) and HepG2-based liver regions of the constructs (identified by lack of RFP) showed typical epithelial phenotype (Fig. 4). These regions showed cells with ZO-1 proteins, β-catenin and vinculin, all markers associated with cell-cell adhesion, with focused expression around the cell membranes. In metastatic regions, highlighted by RFP, ZO-1, β-catenin, and vinculin were generally not expressed along the cell membrane (Figs. 3A,B and 4A–C). This lack of cell-cell binding suggests that the HCT-116 cells had a motile phenotype, which was expected as they had migrated to form these metastases (Gavert and Ben-Ze'ev, 2010; McGrail et al., 2014). Interestingly, there was positive β-catenin staining in the cytoplasmic and nuclear regions of the HCT-116 cells —a phenomenon commonly described in epithelial to mesenchymal transition (EMT) when the WNT/β-catenin pathway is activated. Activation results in β-catenin traveling to the nucleus and acting as a transcription factor that can induce invasive metastatic phenotypes (Behrens, 2000; Brantjes et al., 2002; Orsulic et al., 1999). Additionally, MMP-9, N-cadherin and PCNA stained positive in tumor regions indicating a mesenchymal and proliferative phenotype (Figs. 3C–E and 4D,E; Tania et al., 2014). In comparison, HCT-116 cells cultured on 2-D tissue culture plastic appeared epithelial, showing positive expression of membrane-bound ZO-1 and β-catenin, failing to express N-cadherin (Supplementary Fig. S1), thus supporting the necessity to employ 3-D systems to recapitulate tumor biology with sufficient accuracy. Importantly, the expression of membrane-bound ZO-1 and β-catenin has been shown in 2-D HCT-116 cultures by others (Krubasik et al., 2006), validating our 2-D comparison. Additionally, by transitioning from monolayer culture to spheroid cultures, HCT-116 cells have been shown to show changes of expression of a variety of key markers, including Ki-67, e-cadherin, laminin, p21, and CD44 (Karlsson et al., 2012).

Importantly, these qualitative observations were then quantified; the percentage of HCT116 cells that expressed the markers described above was determined. Figure 5A shows quantification of ZO-1, β-catenin, and N-cadherin in HCT116 cells cultured in 2D on tissue culture plastic. In these cells, membrane-bound ZO-1 and β-catenin expression associated with the cell membrane is present in approximately 95% of the cells, while N-cadherin is limited to only a few select cells. Again, this profile suggests an epithelial phenotype. In contrast, HCT116 cells in both 3D gut and liver constructs show significantly different expression profiles (Fig. 5B,C). Membrane-associated cell–cell adhesions are only present in 10–40% of the HCT116 cells. Conversely N-cadherin is expressed in more than 90% of the HCT116 cells. Statistical comparisons between 2D and 3D gut, and 2D and 3D liver, show significantly different expression percentages for ZO-1, β-catenin, and N-cadherin ($P < 0.01$), verifying the qualitative data observed in the stained sections.

These data indicate that our MOC system provides a facsimile of the logistics that occur during metastasis from the gut to the liver. Furthermore, when we assess the primary tumor sites in the intestine and the metastases in the liver constructs we see evidence of a clear

distinction between metastatic RFP-positive regions and RFP-negative liver regions, which correspond with metastatic/mesenchymal and epithelial marker profiles, respectively.

Tumor Cell Migration in 3-D Responds to Changes in Environmental Mechanical Properties and Drug Treatments

This system, comprised of a tunable hydrogel system, a microperistaltic pump-deriven closed circulatory system, with a reservoir for introducing new media or other substances, and a clear housing for imaging, is a powerful tool for performing system manipulations, investigating biological mechanisms at play, and performing drug testing studies. To demonstrate the utility of this system we have begun performing such experiments. In one application, we have used this platform to explore the influence of physical microenvironment parameters on metastatic invasion. In another application, we have begun employing the MOC system to determine whether established anti-cancer drugs have the same effects in our system as they do in human patients. If this correlation can be expanded and validated, we believe the MOC system can then be robustly implemented in drug candidate screening, and later adapted to personal medicine as a predictive tool by incorporating patient-derived tumor biopsies.

The modular nature of the hydrogel system employed is beneficial as it supports the ability to swap crosslinking agents. Thus, we have control over tissue and tumor elastic modulus ***E'***, or the shear elastic modulus ***G'***, by altering the crosslinker geometry, which changes the effective crosslinking density within the hydrogel network (Skardal et al., 2010d). By using the linear PEGDA crosslinker, hydrogels form with ***G'*** of approximately 100 Pa. However, by using an 8-arm PEG acrylate crosslinker instead, ***G'*** values of approximately 4500 Pa can be achieved (Fig. 6A). Use of a 4-arm crosslinker results in a hydrogel with ***G'*** near 2000 Pa. By employing these 3-D environments in our metastasis platform, we observed that manipulation of these mechanical properties had a profound effect on HCT-116 migratory behavior. HCT-116 tumor foci were created with discrete microenvironment stiffness levels (100 or 4500 Pa) inside of surrounding hydrogel of discrete stiffness (100 or 4500 Pa; Fig. 6B). Figure 6C–E show macro-confocal top-down views, side views, and isometric views of stiff tumor constructs in soft hydrogel (condition 1) or soft tumor constructs in stiff hydrogel (condition 2). In condition 1, we observed some growth of cells near the top interface of the tumors into the surrounding hydrogel. However, in condition 2, we observed migration of large multicellular protrusions and aggregates up and outward from the top of the tumor constructs. This suggests to us that the tissue or tumor stiffness levels can induce or prime tumor cells for increased migratory and invasive behavior, perhaps accelerating metastasis. Additionally, in this increased migratory state, the migrating cells tended to migrate as aggregates rather than single cells. This phenomenon is less pronounced in the alternative condition. Interestingly, it was demonstrated in a mouse model that normal tissue supported invasive metastases, linked to upregulation of the WNT pathway. Conversely, decreased ***E'*** of tissue in a knockout mouse model, in which collagen crosslinking was decreased, the same metastatic tumors failed to metastasize, but grew in their original locations (Levental et al., 2009). This concept of physical parameter influence on tumor invasiveness may give way to new targets of intervention. Perhaps one can artificially induce altered tissue mechanical properties temporarily, thus reducing the likelihood of metastasis. Alternatively,

the physical parameters of tumors and their surrounding environments may serve as biomarkers that are indicative of tumor malignancy and the probability of metastasis.

To demonstrate the use of this system for drug testing, we showed that in the HCT-116 constructs Marimastat can in fact reduce tumor cell invasion into the surrounding environment (Fig. 7). Furthermore, this test also acted as validation of our metastasis observations described in Figure 2, demonstrating that the tumors in the MOC respond as expected to a matrix metalloproteinase inhibiting drug. Tumor constructs were created as described, using the second condition described above (soft tumor [~100 Pa], stiff tissue [~4500 Pa]), which exacerbated metastatic invasion into the surrounding 3-D environment. One half of the prepared systems received normal DMEM, while the other half received 50 μM Marimastat (Sigma) in DMEM. Overlaid fluorescent and brightfield images were captured on day 3, day 7, and day 10, from which distances of migration of cells out of the tumor were determined over time. Figure 7A shows overlays from day 10, illustrating the increased presence of RFP-positive multicellular HCT-116 aggregates moving away from the tumor core in the no drug condition in comparison to the Marimastat group in which fewer RFP-positive cell aggregates are present. Figure 7B depicts the quantification of this migratory activity, in which the no drug control condition shows significantly increased migration distance in microns at each time point. In other words, administration of Marimastat significantly prevented migration of metastatic HCT-116 cells, most likely through inhibition of MMPs (Karakiulakis et al., 1997; Zaman et al., 2006). It should be noted that this experiment was a 10-day snapshot, intended to show that anti-migratory drugs can slow tumor cell migration. Future work will be performed to assess if this treatment truly can prevent migration between the two constructs, or if it simply delays migration.

Additionally, we exposed the HCT-116 constructs to 5-FU, a drug commonly used in colorectal cancer patients that inhibits thymidylate synthase, thereby inducing apoptosis in fast proliferating cancer cells (Macedo and Makarawo, 2014; Wilson et al., 2014). Constructs were cultured for 14 days to establish robust tumor foci, after which they were incubated in four 5-FU concentration (0, 1, 10, and 100 mM) in cell culture media for 24 hours. Measurements of mitochondrial metabolism in the constructs were determined using an MTS assay, which showed a decrease in metabolism with increasing doses of 5-FU (Fig. 7C). However, it should be noted that the measured metabolic rates of the 100 mM-treated groups didn’t differ significantly from the 10 mM-treated groups, suggesting a plateau in drug efficacy. The trend of this data resembles the data we recently showed in a different 3-D liver-colon carcinoma tumor spheroid system, that also responded to 5-FU in a dose dependent manner (Skardal et al., 2015a).

Discussion

These growing sets of 3-D drug testing data indicate that our system, and those developed by others, are becoming more capable of recapitulating the desired, human-mimicking, and nuanced responses to drug treatments. There is a rapidly growing push to shift the paradigm of 2-D drug screening platforms to more advanced 3-D systems. Experiments such as those described here make a strong argument for such a shift.

The concept of a MOC system using 3-D constructs addresses many current shortcomings in cancer research. First and foremost, animal models are not optimal for quick studies and high-throughput scenarios because of the often long experimental time courses and the difficulty of scaling study sizes. They only support the capability for limited mechanistic manipulation and do not always offer simple ways to monitor the results. Perhaps, most importantly, results in animals are not necessarily predictive of results in humans. The other most common tool in cancer research, traditional 2-D cultures, fails to recapitulate the 3-D microenvironment of in vivo tissues (Kunz-Schughart et al., 2004). For a number of reasons, the drug doses that are found to be effective in 2-D are often less effective when scaled to patients (Drewitz et al., 2011; Ho et al., 2010). The MOC system addresses these problems by using human-derived cells and employing them in a 3-D hydrogel-supported environment. We observed appropriate cell-cell interactions depending on host tissue or tumor regions, and the tumors respond appropriately to an anti-migratory drug. Another lacking aspect in many research approaches is failure to consider both the primary tumors site and the downstream site, or sites, of metastasis. The MOC was conceptualized to specifically include tissue-engineered 3-D constructs representing these multiple sites, allowing researchers to begin to recapitulate the kinetics of certain aspects of metastatic migration from an originating tissue to a target tissue. This is both important and novel because the phenotype of cells in the originating tumors and the metastases can vary significantly (Franci et al., 2013; Karakiulakis et al., 1997). Having the ability to study both tumor types and microenvironments is integral to accurately model metastasis in its entirety. Our system successfully supports tumor growth in primary site constructs over time. The metastatic colon carcinoma cells we employed, HCT-116, were capable of breaking out of the construct and then entering circulation. Furthermore, and importantly, the circulating cells reached the downstream construct within the device, invading the construct's 3-D space, and continuing to grow in size. This is consistent with a liver-tumor spheroid-based construct model we developed recently, in which the metastatic tumor grew over time within the liver host tissue (Skardal et al., 2015a). Also notable was the fact that when we employed a less metastatic cell type, SW480 cells, they failed to migrate to the liver construct, instead remaining in the gut construct while proliferating. Importantly, immunostaining data from this and the previously referenced study both demonstrate a clear distinction between the epithelial construct environment and mesenchymal marker-expressing tumor foci. Notably, this is dramatically different from when HCT-116 cells are cultured on traditional 2-D tissue culture plastic, where they appear epithelial instead of mesenchymal and metastatic in nature. The data we have described here is a collection of the first validation and verification experiments performed with the system. We also demonstrated the ability to manipulate the system using modular hydrogel technology to create tumor microenvironment changes or by administering chemotherapy drugs, after which the effects of these factors were able to be observed and documented in a straightforward fashion, thus demonstrating the significant potential that we believe this platform possesses to be used in a multitude of mechanistic and screening applications.

Despite the findings we showcase here, we also recognize several limitations of the current generation of our MOC system. The constructs we have employed have a simplistic architecture. As described above, the method for biofabrication of these constructs and the

tumor foci within is by simply encapsulating cells within hydrogel and photopolymerizing them without true control over cellular location. Fortunately, in the constructs we describe here, this appears to sufficient. We observe growing tumor foci, tumor regions that disseminate into the circulating media, and reach a downstream construct site, further growing into another tumorigenic mass. However, we wish to employ the constructs as complete functional mimics of their in vivo counterparts, allowing us to assess the impacts of tumor growth as well as drugs and other therapeutic agents on not only the tumors, but the general health and functionality of the host tissues. Simple cell encapsulation may not be suitable for such recapitulation of real in vivo-like function. Additionally, this reductionist model does not include an endothelial component, which is an important aspect of true metastasis. Incorporating an endothelial barrier, through which the tumor cells must intravasate and extravasate is a next step in our work. We also do not currently have an immune component in the system, which is another important feature to consider. Fortunately, our team has experience in a number biofabrication technologies such as bioprinting, and many of them incorporate the very hydrogel system described here, modified to support 3-D extrusion protocols. Using such biofabrication techniques (Murphy et al., 2013; a,b,c,d, 2012), we are working to create more intricate structures that will better mirror the architecture of human tissues, as well as their function. We are also transitioning to implementation of more optimal cell types. We already have experience working with primary human hepatocytes for creating liver constructs (Lang et al., 2011; Skardal et al., 2012), and in currently unpublished work, our team is working with primary cells and induced pluripotent stem cells to create highly functioning constructs of various tissue types for an integrated multi-construct system. Integrating this work with our MOC platform and biofabrication strategies has the potential to achieve high functioning, cell line-free constructs with biologically inspired architecture. Furthermore, if we can adapt our system to employ patient-specific cells, we will have a powerful tool for use in a number of arenas, including drug and toxicology screening, identification of targets of intervention, and predictive platforms for individual patients.

Conclusions

With an ever-increasing need for physiologically accurate platforms for more accurate modeling of cancer and more efficient drug development and screening, the MOC system presented here has the potential to serve as powerful tool in the hands of researchers. This system supports some aspects of the logistical phenomena of metastasis, allowing study of the translocation of metastatic tumor cells from a primary tissue site to a downstream tissue site. Moreover, the tumor constructs in the system can be manipulated in a variety of methods, demonstrated by several experiments that began to assess the influences of tissue and tumor mechanical properties as well as an established anti-migratory drug on tumor cell migration. We also envision adaptation of this in vitro metastasis model to other tissue types, with additional components such as endothelial barriers and more functional host cells, which will allow extensive investigation of many cancer varieties and exploration of the complex mechanisms at play during metastasis, and ultimately providing a powerful platform for use in future drug screening, toxicology studies, and personalized medicine.

Supplementary Material

Refer to Web version on PubMed Central for supplementary material.

Acknowledgments

Contract grant sponsor: Golfers Against Cancer

Contract grant sponsor: Comprehensive Cancer Center of Wake Forest Baptist Medical Center

Contract grant sponsor: Wake Forest Institute for Regenerative Medicine Promoting Innovating Discoveries Funding Program

References

Allison DD, Grande-Allen KJ. Review. Hyaluronan: a powerful tissue engineering tool. Tissue Eng. 2006; 12(8):2131–2140. [PubMed: 16968154]

Behrens J. Control of beta-catenin signaling in tumor development. Ann N Y Acad Sci. 2000; 910:21–33. [PubMed: 10911903]

Benam KH, Dauth S, Hassell B, Herland A, Jain A, Jang KJ, Karalis K, Kim HJ, MacQueen L, Mahmoodian R, Musah S, Torisawa YS, van der Meer AD, Villenave R, Yadid M, Parker KK, Ingber DE. Engineered in vitro disease models. Annu Rev Pathol. 2015; 10:195–262. [PubMed: 25621660]

Brantjes H, Barker N, van Es J, Clevers H. TCF: Lady Justice casting the final verdict on the outcome of Wnt signalling. Biol Chem. 2002; 383(2):255–261. [PubMed: 11934263]

Burdick JA, Prestwich GD. Hyaluronic acid hydrogels for biomedical applications. Adv Mater. 2011; 23(12):H41–H56. [PubMed: 21394792]

Drewitz M, Helbling M, Fried N, Bieri M, Moritz W, Lichtenberg J, Kelm JM. Towards automated production and drug sensitivity testing using scaffold-free spherical tumor microtissues. Biotechnol J. 2011; 6(12):1488–1496. [PubMed: 22102438]

Fidler IJ, Kim SJ, Langley RR. The role of the organ microenvironment in the biology and therapy of cancer metastasis. J Cell Biochem. 2007; 101(4):927–936. [PubMed: 17177290]

Franci C, Zhou J, Jiang Z, Modrusan Z, Good Z, Jackson E, Kouros-Mehr H. Biomarkers of residual disease, disseminated tumor cells, and metastases in the MMTV-PyMT breast cancer model. PLoS ONE. 2013; 8(3):e58183. [PubMed: 23520493]

Gavert N, Ben-Ze'ev A. Coordinating changes in cell adhesion and phenotype during EMT-like processes in cancer. F1000 Biol Rep. 2010; 2:86. [PubMed: 21283595]

Ho WJ, Pham EA, Kim JW, Ng CW, Kim JH, Kamei DT, Wu BM. Incorporation of multicellular spheroids into 3-D polymeric scaffolds provides an improved tumor model for screening anticancer drugs. Cancer Sci. 2010; 101(12):2637–2643. [PubMed: 20849469]

Karakiulakis G, Papanikolaou C, Jankovic SM, Aletras A, Papakonstantinou E, Vretou E, Mirtsou-Fidani V. Increased type IV collagen-degrading activity in metastases originating from primary tumors of the human colon. Invasion Metastasis. 1997; 17(3):158–168. [PubMed: 9702942]

Karlsson H, Fryknas M, Larsson R, Nygren P. Loss of cancer drug activity in colon cancer HCT-116 cells during spheroid formation in a new 3-D spheroid cell culture system. Exp Cell Res. 2012; 318(13):1577–1585. [PubMed: 22487097]

Krubasik D, Iyer NG, English WR, Ahmed AA, Vias M, Roskelley C, Brenton JD, Caldas C, Murphy G. Absence of p300 induces cellular phenotypic changes characteristic of epithelial to mesenchyme transition. Br J Cancer. 2006; 94(9):1326–1332. [PubMed: 16622451]

Kunz-Schughart LA, Freyer JP, Hofstaedter F, Ebner R. The use of 3-D cultures for high-throughput screening: the multicellular spheroid model. J Biomol Screen. 2004; 9(4):273–285. [PubMed: 15191644]

Lang R, Stern MM, Smith L, Liu Y, Bharadwaj S, Liu G, Baptista PM, Bergman CR, Soker S, Yoo JJ, Atala A, Zhang Y. Three-dimensional culture of hepatocytes on porcine liver tissue-derived extracellular matrix. Biomaterials. 2011; 32(29):7042–7052. [PubMed: 21723601]

Langley RR, Fidler IJ. Tumor cell-organ microenvironment interactions in the pathogenesis of cancer metastasis. Endocr Rev. 2007; 28(3):297–321. [PubMed: 17409287]

Levental KR, Yu H, Kass L, Lakins JN, Egeblad M, Erler JT, Fong SF, Csiszar K, Giaccia A, Weninger W, Yamauchi M, Gasser DL, Weaver VM. Matrix crosslinking forces tumor progression by enhancing integrin signaling. Cell. 2009; 139(5):891–906. [PubMed: 19931152]

Macedo FI, Makarawo T. Colorectal hepatic metastasis: Evolving therapies. World J Hepatol. 2014; 6(7):453–463. [PubMed: 25067997]

McGrail DJ, Mezencev R, Kieu QM, McDonald JF, Dawson MR. SNAIL-induced epithelial-to-mesenchymal transition produces concerted biophysical changes from altered cytoskelgene expression. FASEB J. 2014; 29(4):1280–1289. [PubMed: 25491311]

Murphy SV, Skardal A, Atala A. Evaluation of hydrogels for bio-printing applications. J Biomed Mater Res A. 2013; 101(1):272–284. [PubMed: 22941807]

Orsulic S, Huber O, Aberle H, Arnold S, Kemler R. E-cadherin binding prevents beta-catenin nuclear localization and beta-catenin/LEF-1-mediated transactivation. J Cell Sci. 1999; 112(Pt 8):1237–1245. [PubMed: 10085258]

Polini A, Prodanov L, Bhise NS, Manoharan V, Dokmeci MR, Khademhosseini A. Organs-on-a-chip: a new tool for drug discovery. Expert Opin Drug Discov. 2014; 9(4):335–352. [PubMed: 24620821]

Prestwich GD, Kuo JW. Chemically-modified HA for therapy and regenerative medicine. Curr Pharm Biotechnol. 2008; 9(4):242–245. [PubMed: 18691083]

Prestwich GD. Simplifying the extracellular matrix for 3-D cell culture and tissue engineering: a pragmatic approach. J Cell Biochem. 2007; 101(6):1370–1383. [PubMed: 17492655]

Prestwich GD. Evaluating drug toxicity and efficacy in three dimensions: Using synthetic extracellular matrices in drug discovery. Acc Chem Res. 2008; 41:139–148. [PubMed: 17655274]

Prestwich GD. Hyaluronic acid-based clinical biomaterials derived for cell and molecule delivery in regenerative medicine. J Control Release. 2011; 155(2):193–199. [PubMed: 21513749]

Skardal A, Sarker SF, Crabbe A, Nickerson CA, Prestwich GD. The generation of 3-D tissue models based on hyaluronan hydrogel-coated microcarriers within a rotating wall vessel bioreactor. Biomaterials. 2010a; 31(32):8426–8435. [PubMed: 20692703]

Skardal A, Zhang J, McCoard L, Oottamasathien S, Prestwich GD. Dynamically crosslinked gold nanoparticle—hyaluronan hydrogels. Adv Mater. 2010b; 22(42):4736–4740. [PubMed: 20730818]

Skardal A, Zhang J, McCoard L, Xu X, Oottamasathien S, Prestwich GD. Photocrosslinkable hyaluronan-gelatin hydrogels for two-step bioprinting. Tissue Eng Part A. 2010c; 16(8):2675–2685. [PubMed: 20387987]

Skardal A, Zhang J, Prestwich GD. Bioprinting vessel-like constructs using hyaluronan hydrogels crosslinked with tetrahedral polyethylene glycol tetracrylates. Biomaterials. 2010d; 31(24):6173–6181. [PubMed: 20546891]

Skardal A, Smith L, Bharadwaj S, Atala A, Soker S, Zhang Y. Tissue specific synthetic ECM hydrogels for 3-D in vitro maintenance of hepatocyte function. Biomaterials. 2012; 33(18):4565–4575. [PubMed: 22475531]

Skardal A, Devarasetty M, Rodman C, Atala A, Soker S. Liver-tumor hybrid organoids for modeling tumor growth and drug response in vitro. Ann Biomed Eng. 2015a; 43(10):2361–2373. [PubMed: 25777294]

Skardal A, Devarasetty M, Soker S, Hall AR. In situ patterned micro 3D liver constructs for parallel toxicology testing in a fluidic device. Biofabrication. 2015b; 7(3):031001. [PubMed: 26355538]

Tania M, Khan MA, Fu J. Epithelial to mesenchymal transition inducing transcription factors and metastatic cancer. Tumour Biol. 2014; 35(8):7335–7342. [PubMed: 24880591]

Wilson PM, Danenberg PV, Johnston PG, Lenz HJ, Ladner RD. Standing the test of time: targeting thymidylate biosynthesis in cancer therapy. Nat Rev Clin Oncol. 2014; 11(5):282–298. [PubMed: 24732946]

Xia Y, Whitesides GM. Soft lithography. Annu Rev Mater Sci. 1998; 28:153–184.

Zaman MH, Trapani LM, Sieminski AL, Mackellar D, Gong H, Kamm RD, Wells A, Lauffenburger DA, Matsudaira P. Migration of tumor cells in 3D matrices is governed by matrix stiffness along with cell-matrix adhesion and proteolysis. Proc Natl Acad Sci USA. 2006; 103(29):10889–10894. [PubMed: 16832052]

Zhang J, Skardal A, Prestwich GD. Engineered extracellular matrices with cleavable crosslinkers for cell expansion and easy cell recovery. Biomaterials. 2008; 29(34):4521–4531. [PubMed: 18768219]

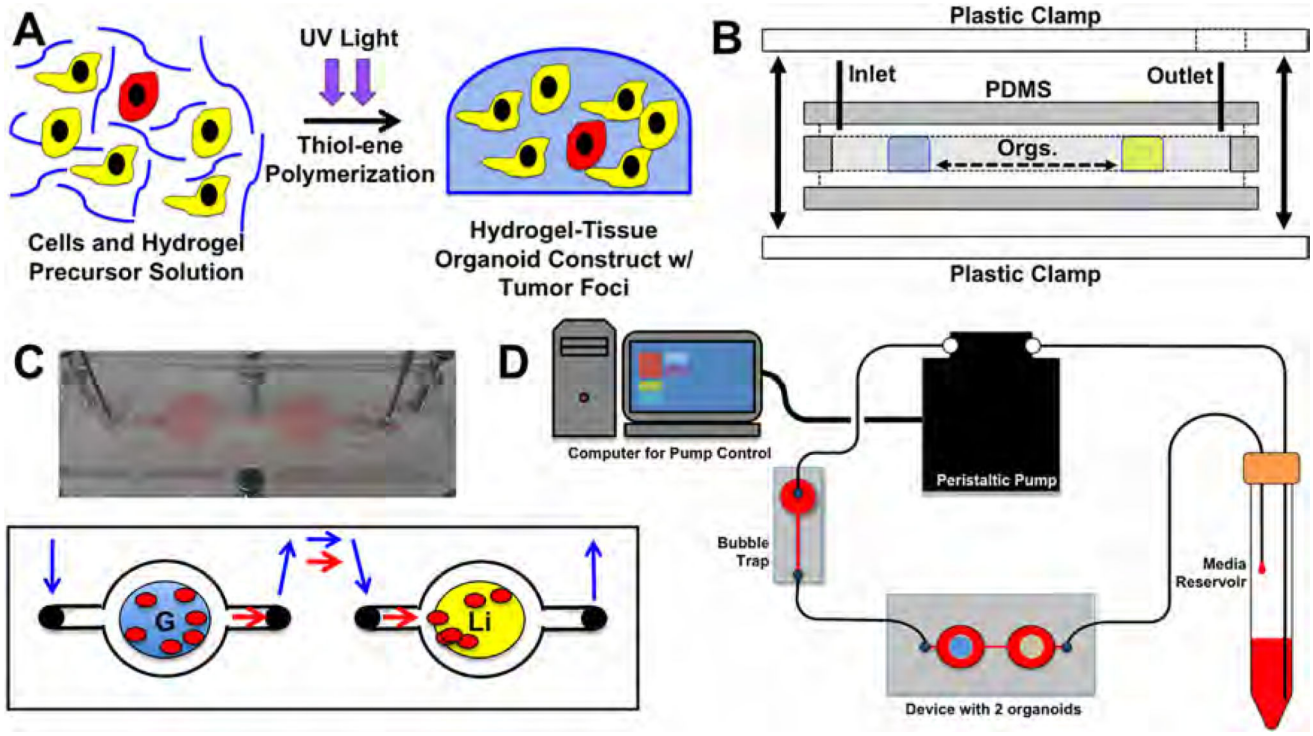

Figure 1.

The 2-construct “metastasis-on-a-chip” device and fluidic platform for mimicking colon carcinoma metastasis from the gut to the liver. **A:** Photopolymerization of cells in a polymer solution forms 3-D tissue constructs. **B:** Device fabrication using molded PDMS pieces, inlet and outlet valves, and plastic clamps. Construct placement (“Orgs.”) is indicated by the blue and yellow zones. **C:** Photo and depiction of the device, and gut and liver constructs in the device under flow with migrating cancer cells. Blue arrows—direction of tissue culture media flow; Red arrows—direction of potential migration of tumor cells between constructs. **D:** The MOC device inline with media reservior, bubble trap, and micro-peristaltic pump, providing circulatory flow in the gut-to-liver direction.

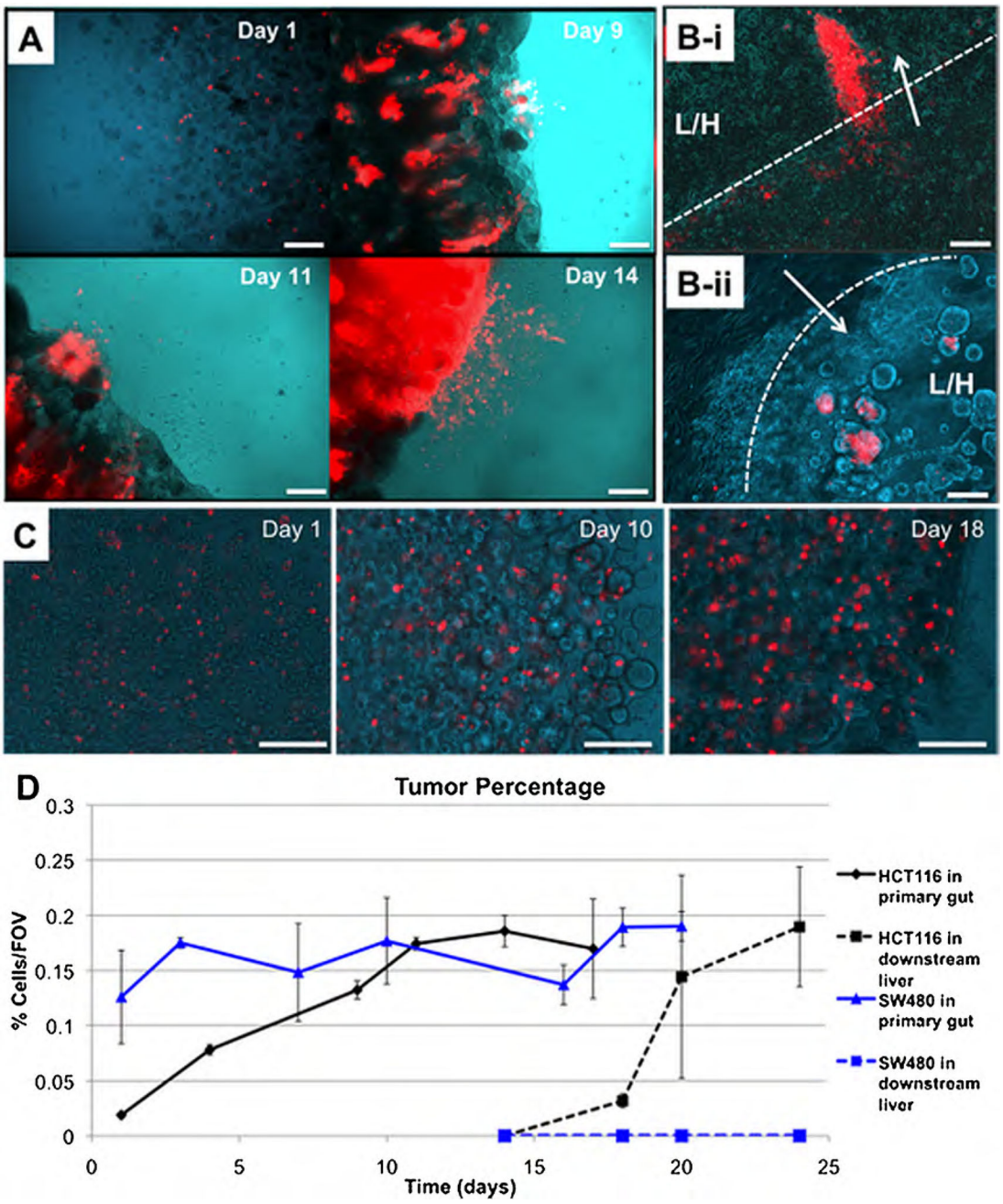

Figure 2.

HCT-116 colon carcinoma cells metastasize from the gut to the liver, while less malignant SW480 colon carcinoma cells do not. **A:** Growth of HCT-116 cells in the primary gut construct, and subsequent shedding of RFP-labeled HCT-116 cells into circulation. **B:** (i–ii) Invasion of RFP-labeled HCT116 cells into liver constructs, via multicellular protrusions and aggregates invading a liver-hydrogel construct. (Arrow—direction of invasion; Dotted line—construct interface; L/H—liver/hydrogel construct). **C:** SW480 cells grow in the primary construct, but never appear to shed into circulation or colonize the downstream liver construct. **D:** Quantification of the relative area per field of view occupied by HCT-116 cells

(Black lines) and SW480 cells (Blue lines). Solid lines indicate quantification in the primary gut construct and dashed lines indicate quantification in the downstream liver construct. Scale bars—250 μm.

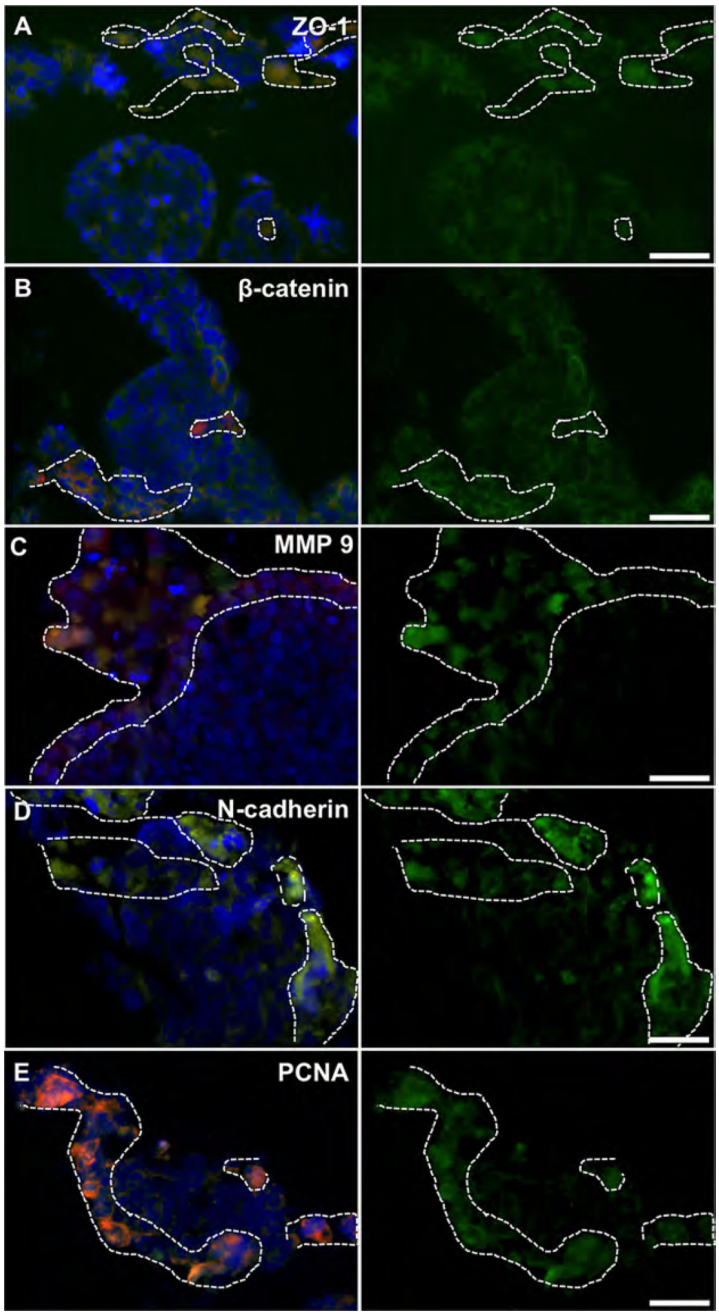

Figure 3.

Marker expression of RFP-labeled HCT-116 tumor cells (dashed line) inside 3-D intestine constructs. HCT-116 regions do not clearly express membrane-bound (**A**) ZO-1, or (**B**) β-catenin, indicating a more motile phenotype. β-catenin accumulates in the cytoplasm/nucleus suggesting WNT pathway activation, common in metastatic cells after epithelial-to-mesenchymal transition. RFP-labeled HCT-116 cells express (**C**) MMP-9, (**D**) N-cadherin, and (**E**) PCNA indicating a mesenchymal and metastatic proliferative phenotype. Conversely, intestine epithelial regions (no RFP) exhibit traditional epithelial phenotype with membrane-bound ZO-1, and β-catenin, while expressing MMP-9, N-cadherin and

PCNA less strongly. Green—indicated stain; Red—RFP-labeled HCT-116 cells; Blue—DAPI. Scale bars—50 μm. Dotted white lines outline RFP+ HCT-116 rich regions.

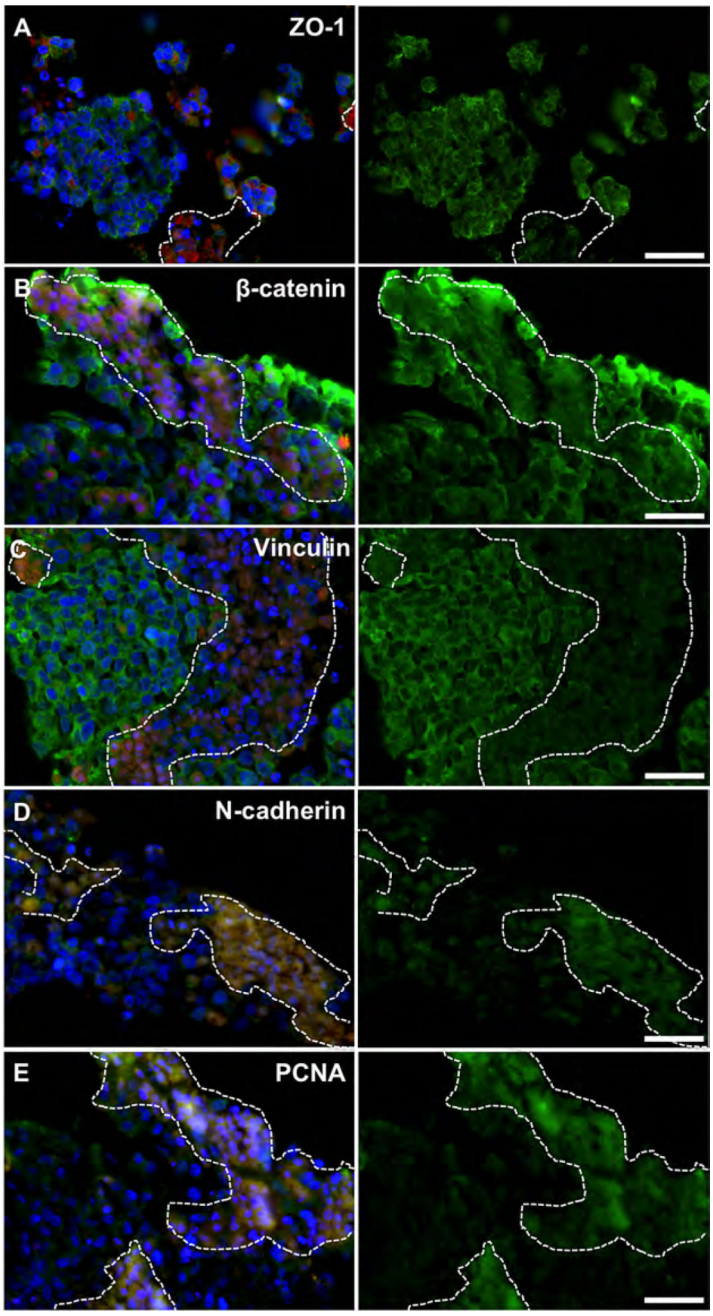

Figure 4.

Marker expression of RFP-labeled HCT-116 metastases (dashed line) inside 3-D liver constructs. HCT-116 regions do not clearly express membrane-bound (**A**) ZO-1, **B**) β-catenin, or **C**) vinculin, indicating a more motile phenotype. β-catenin accumulates in the cytoplasm/nucleus suggesting WNT pathway activation, common in metastatic cells after epithelial-to-mesenchymal transition. RFP-labeled HCT-116 cells express (**D**) N-cadherin and (**E**) PCNA indicating a mesenchymal and metastatic proliferative phenotype. Conversely, HepG2 regions (no RFP) exhibit traditional epithelial phenotype with membrane-bound ZO-1, β-catenin, and vinculin, while expressing N-cadherin and PCNA

less strongly. Green—indicated stain; Red—RFP-labeled HCT-116 cells; Blue—DAPI. Scale bars—50 μm. Dotted white lines outline RFP+ HCT-116 rich regions.

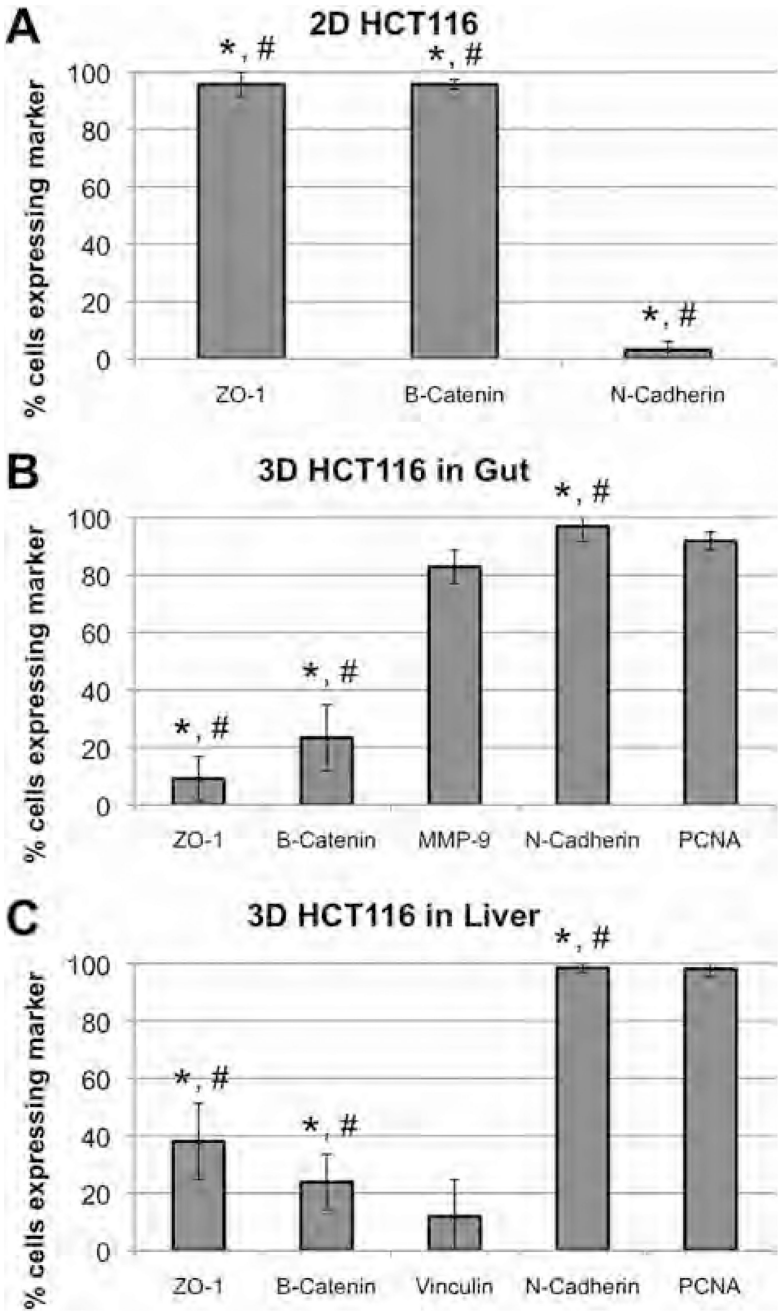

Figure 5.

Marker quantification of HCT-116 cells in 2D culture, in 3D gut constructs, and 3D liver constructs. **A:** In 2D culture on tissue culture plastic, HCT116 cells express high levels of cell-cell adhesion markers such as membrane-bound ZO-1 and β-catenin, while expressing very little N-cadherin, a mesenchymal marker. **B:** In the primary construct site, the gut, HCT116 cells express low levels of ZO-1 and β-catenin, while expressing high levels of MMP9, N-cadherin, and PCNA. **C:** Similarly, in the metastases sites in the liver, HCT116 cells also express low levels of ZO-1, β-catenin, and vinculin, while expressing high levels of N-cadherin and PCNA. Statistical significance: $*P < 0.01$ between corresponding markers

in 2D versus gut constructs; #$P < 0.01$ between corresponding markers in 2D versus liver constructs.

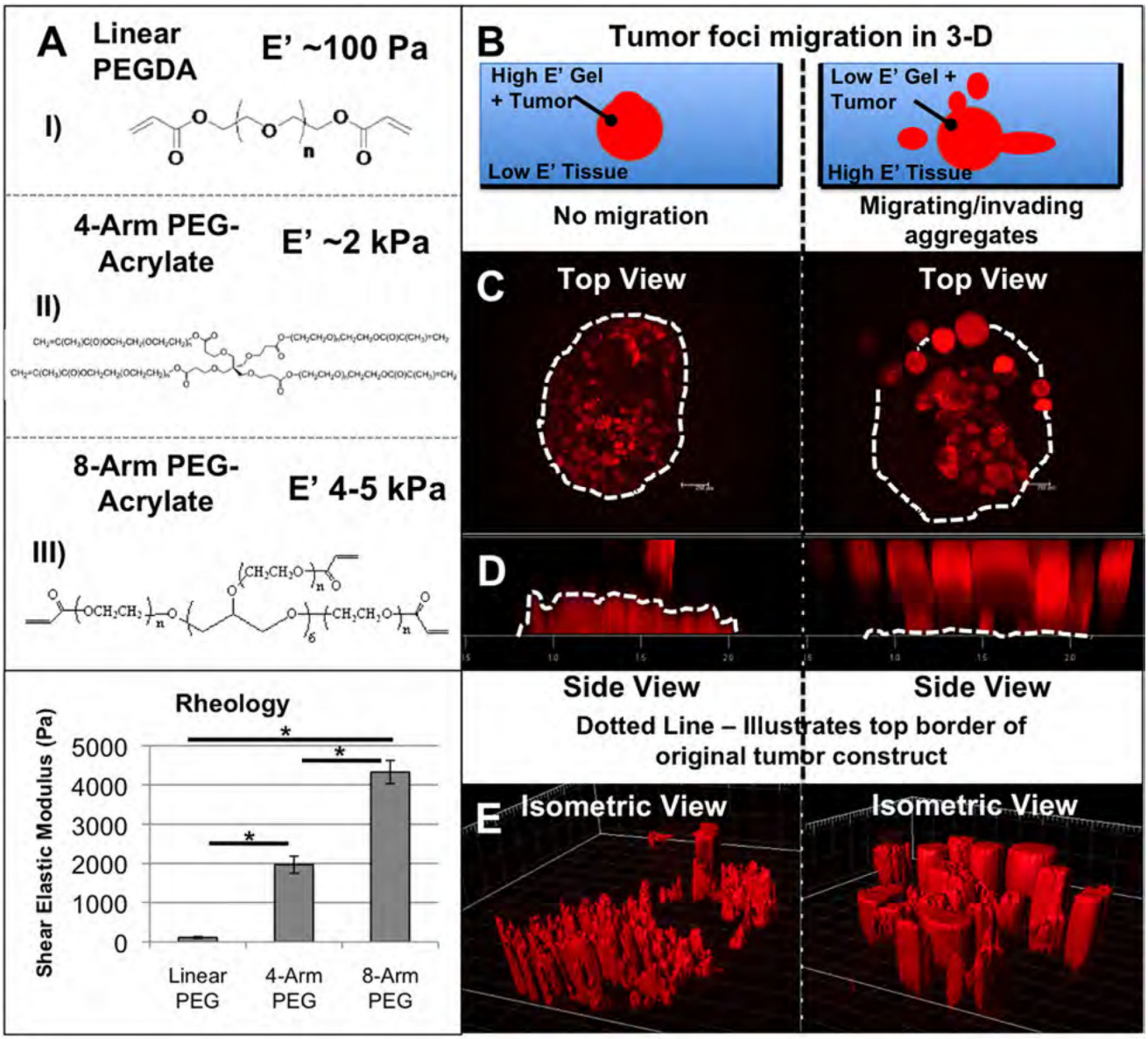

Figure 6.

The effect of tissue and tumor microenvironment elastic modulus on metastatic migration of HCT116 cells in 3-D. **A:** Using acrylate-functionalized PEG-based crosslinkers of varying geometry allows for manipulation of hydrogel-based construct and tumor mechanical properties. Rheological data demonstrates statistically different (*$P < 0.05$) shear elastic moduli of hydrogels created using these crosslinkers. **B:** HCT116 cells were embedded in a central stiff gel core of 4.5 kPa surrounded by soft 100 Pa hydrogel-based tissue construct (left), or in a soft 100 Pa core surrounded by a stiff 4.5 kPa hydrogel-based tissue construct (right). **C:** Top-down, **D**) side, and (**E**) isometric macroconfocal images of tumors and space above the tumors. Stiff-core, soft environment tumors grow, but remain primarily at the tumor's location. Soft-core, stiff environment tumors exhibit increased migration outwards

from the tumor into the stiff environment in the form of large multicellular protrusions and aggregates.

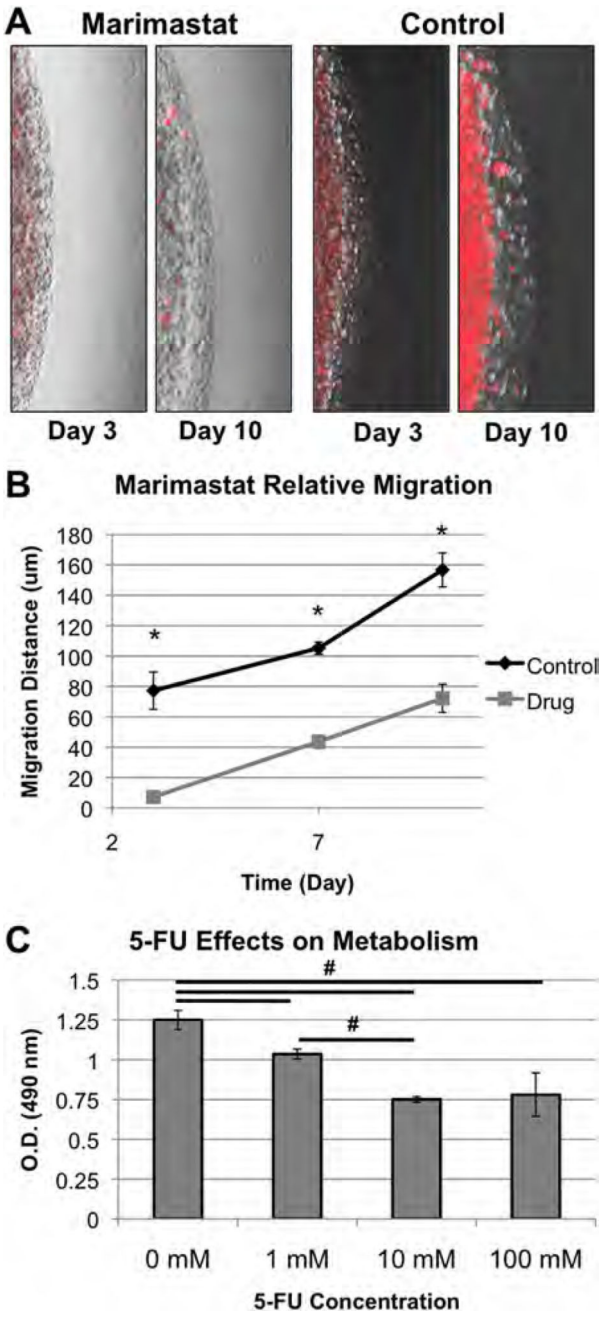

Figure 7.

Performing drug testing in the metastasis-on-a-chip device. **A–B:** The effects of Marimastat on HCT-116 migration. **A:** Marimastat prevents outward growth of aggregates from HCT-116 tumor constructs in 3-D, while control conditions do not. **B:** Migration of HCT-116 cells quantified by length in pixel counts. Significance: $*P < 0.05$ between experimental groups at each time point. **C:** HCT-116 tumor constructs respond in a dose dependent manner to 5-Fluorouracil (5-FU). MTS assays quantified the effects of 48-h 0, 1,

10, and 100 mM 5-Fluorouracil treatments on the mitochondrial metabolism of the HCT-116 tumor constructs. Significance: #$P < 0.05$ between the indicated groups.